# Broadband CPW Feed for Millimeter-Wave SIW-Based Antipodal Linearly Tapered Slot Antennas

Farzaneh Taringou, *Student Member, IEEE*, David Dousset, Jens Bornemann, *Fellow, IEEE*, and Ke Wu, *Fellow, IEEE*

***Abstract*—To achieve broadband performances in the millimeter-wave range, antipodal linearly tapered slot antenna (ALTSA) designs with new combined substrate integrated waveguide (SIW) and regular coplanar waveguide (CPW) feeds are presented and studied. This feed structure eliminates the fabrication of air bridges in direct CPW-fed tapered slot antennas (TSAs). Two millimeter-wave design techniques are introduced for the selected 41–61 GHz and 90–120 GHz frequency ranges, demonstrating very good impedance match and nearly constant gain, beamwidth, and cross-polarization levels over bandwidths of 39% and 28%, respectively. The design procedure is validated by comparing simulated results with measurements performed on a 21–31 GHz (38% bandwidth) prototype. Very good agreement between measured and calculated performance characteristics is obtained with only cross-polarization levels slightly higher than predicted. The structural design parameters and dimensions of all three designs are given.**

***Index Terms*—Antenna feeds, broadband antennas, coplanar waveguides, Vivaldi antennas, waveguide transitions.**

## I. Introduction

DUE to its end-fire characteristics, wide bandwidth, and ease of fabrication, the printed tapered slot antenna (TSA) [1], [2] has found numerous applications in arrays [3], phased and scanning arrays [4], and dual-polarized focal-plane imaging systems [5]. Its uni-planar version has excellent polarization performance that has been demonstrated for frequencies in the millimeter-wave [6] and terahertz ranges [7].

The profile of a TSA, either in exponential or linearly tapered form, is well known, and so are principal design guidelines, basic gain, and radiation pattern and cross-polarization characteristics. Numerous papers have appeared on this subject, e.g., [8]–[13], and thus the topic of this paper is not concerned with the reinvention of the TSA.

Manuscript received April 27, 2012; revised April 27, 2012; accepted November 21, 2012. Date of publication December 10, 2012; date of current version April 03, 2013. This work was supported by the Natural Science and Engineering Research Council of Canada.

F. Taringou and J. Bornemann are with the Department of Electrical and Computer Engineering, University of Victoria, Victoria, BC V8N 0A6, Canada (e-mail: ftaringo@uvic.ca; j.bornemann@ieee.org).

D. Dousset and K. Wu are with the Poly-Grames Research Center, Department of Electrical Engineering, École Polytechnique de Montreal, Montreal, QC H3C 3A7, Canada (e-mail: david.dousset@polymtl.ca; ke.wu@ieee.org).

Color versions of one or more of the figures in this paper are available online at http://ieeexplore.ieee.org.

Digital Object Identifier 10.1109/TAP.2012.2232270

However, the challenge usually lies in the selection of an appropriate feed for the TSA, which is in connection with the new contribution of this work. A common feed for the TSA consists of using a microstrip-to-slotline transition [4], [5] where the microstrip line is positioned on one side of the substrate and the slot, feeding the TSA, on the other. Such transitions are usually bandwidth-limited as they incorporate frequency-dependent transition elements.

The direct connection to a microstrip line requires the TSA to become an antipodal TSA (ATSA) such that the field in the microstrip line, which is oriented perpendicular to the substrate, can be rotated to lie in the plane of the substrate [8]–[13]. This method not only results in extremely broadband performance [10] but also, with added corrugations, contributes to better return loss, higher gain, and better cross-polarization performance [13].

Nowadays, substrate integrated waveguide (SIW) technology, e.g., [14], has been widely accepted as an excellent compromise between microstrip and all-metal waveguide circuitry. The field rotation between SIW and the ATSA is similar to that of the microstrip feed. However, the SIW losses at millimeter-wave frequencies are an order of magnitude lower than those of the microstrip line, or, conversely, the unloaded quality factor of an SIW resonator is an order of magnitude higher than that of a microstrip resonator [15]. Thus, a number of ATSAs have been proposed that incorporate SIW feeding technology. For measurement and/or modeling purposes, however, the microstrip line remains, but it is now connected to the SIW instead of the ATSA directly [15]–[19].

It is well known that, for millimeter-wave integrated circuits, coplanar waveguide (CPW) technology has several advantages over microstrip lines which include surface-mount integration, lower phase velocity variation, lower cross talk, and radiation [20], [21]. Therefore, a case can be made that millimeter-wave TSAs or ATSAs would rather be fed by CPWs than microstrip. Such an approach is presented in [22] and [23]. However, the feeding line in these papers is a grounded CPW (GCPW), which could contribute to the limitation of bandwidth due to the excitation of waveguide-type modes [24] over the band of interest. Moreover, the bandwidth of these designs is relatively small, and cross-polarization issues remain unaccounted for.

Therefore, this paper presents a new broadband CPW feed for SIW-based antipodal linearly tapered slot antennas (ALTSAs). The advantage of this feed is that it avoids bond wires and/or air bridges [25], [26], whose fabrication complexity hinders a direct connection between a regular CPW and TSA or ATSA. Two millimeter-wave designs for 41–61 GHz and 90–120 GHz

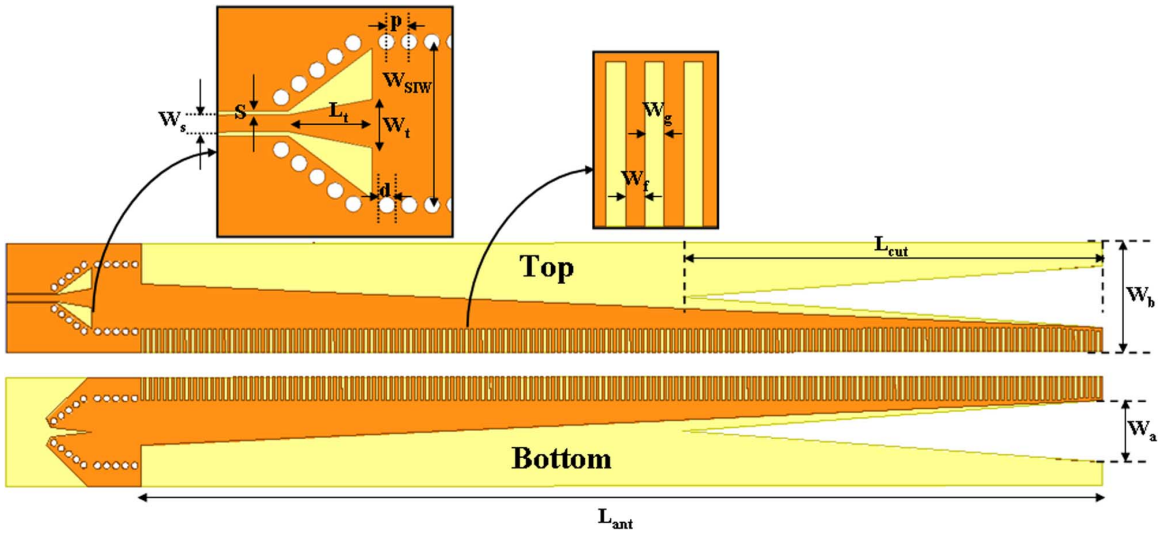


Fig. 1. Top and bottom (as seen from the top) views of SIW-based ALTSA with broadband CPW feed and dimensional parameters.

are presented to demonstrate feasible broadband CPW-fed ALTSA operation and to provide the antenna engineer with dimensional parameters for future SIW-based antenna systems. The design procedure is experimentally verified by prototype measurements between 21 and 31 GHz.

## II. Design Technique

Fig. 1 shows a sketch of the SIW-based ALTSA with broadband CPW feed, including its main design parameters. The frequency range is determined by the SIW circuit whose equivalent waveguide width is determined by

$$a_{\mathrm{equ}} = \frac{c}{2 f_c \sqrt{\varepsilon_r}} \tag{1}$$

where $c$ is the speed of light, $f_c$ the desired cutoff frequency of the SIW, and $\varepsilon_r$ is the substrate's permittivity. The width $W_{\mathrm{SIW}}$ of the SIW (cf. Fig. 1) is obtained from a number of published approaches that provide very accurate values, depending on the ratio of the via diameter to spacing $d/p$, as presented in [27]. Note that a $d/p$ ratio of 0.5 or higher is recommended in practice to avoid leakage through the vias.

The second design step involves the ALTSA for which several previously published guidelines are utilized. According to [2], the condition for the aperture opening is

$$W_a \geq \lambda_0/2 \tag{2}$$

and the effective thickness has to satisfy

$$0.005 < \frac{t_{\mathrm{eff}}}{\lambda_0} < 0.03, \quad t_{eff} = (\sqrt{\varepsilon_r} - 1)\, b \tag{3}$$

where $b$ is the substrate thickness. For the antenna length, [28] recommends

$$3\lambda_0 < L_{\mathrm{ant}} < 8\lambda_0. \tag{4}$$

In (2)–(4), $\lambda_0$ refers to the free-space wavelength at the center frequency of the operating bands, which are, according to Table I, 26, 51, and 105 GHz, respectively. When considering the length of the antenna, certain substrate thickness is required for stability reasons. This usually leads to the violation of (3). Therefore, it is common to cut a certain amount of the substrate, e.g. parameter $L_{\mathrm{cut}}$ in Fig. 1, to lower $\varepsilon_r$ in the aperture and thus satisfy (3).

TABLE I
Dimensions [in mm] According to Fig. 1

| Parameter | 21-31 GHz | 41-61 GHz | 90-120 GHz |
|---|---|---|---|
| $\varepsilon_r$ | 2.94 | 2.94 | 2.94 |
| $b$ | 0.508 | 0.254 | 0.127 |
| $W_a$ | 5.8 | 3.02 | 1.41 |
| $W_b$ | 10.2 | 5.02 | 2.29 |
| $L_{ant}$ | 89.5 | 45.0 | 30.0 |
| $L_{cut}$ | 39.0 | 22.0 | 9.5 |
| $W_f$ | 0.26 | 0.13 | 0.14 |
| $W_g$ | 0.26 | 0.13 | 0.14 |
| $W_{SIW}$ | 6.27 | 3.5 | 1.8 |
| $d$ | 0.62 | 0.62 | 0.4 |
| $p$ | 0.86 | 0.86 | 0.65 |
| $W_t$ | 1.85 | 1.1 | 0.7 |
| $L_t$ | 3.21 | 1.45 | 1.17 |
| $W_s$ | 0.65 | 0.76 | 0.64 |
| $s$ | 0.15 | 0.2 | 0.15 |
| $Z_0$ | 68 Ω | 75 Ω | 75 Ω |

In order to reduce cross-polarization levels, and at the same time reduce the overall height $W_b$ of the antenna [29], corrugations are employed in the upper and lower fins of the ALTSA. Their dimensions are obtained from scaled values of the 60-GHz design in [29] in which the corrugations reduce the antenna height above and below the aperture, $(W_b - W_a)/2$, by a factor of four compared to an antenna without corrugations. The beneficial influence of the corrugations on input return loss, gain, and especially cross-polarization levels is presented in [13].

The third design step concerns the CPW-to-SIW transition at the antenna input. It is based on a slight modification of a very recent design exercise in [24]. The SIW is first connected to a quasi-microstrip line of length $L_t$ and width $W_t$ whose initial dimensions are chosen according to an SIW-to-microstrip taper

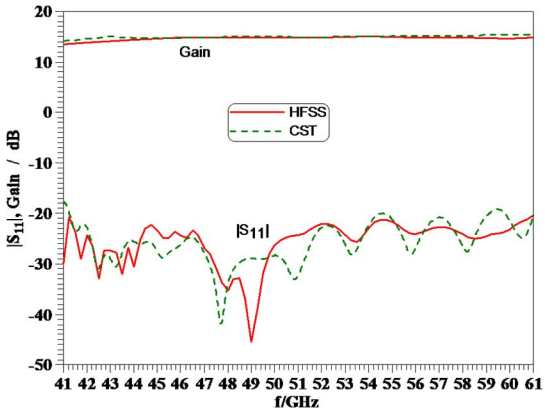


Fig. 2. Input reflection coefficient and gain in dB of the 41–61-GHz ALTSA and comparison between HFSS and CST.

as presented in [30]. However, its bottom metallization is gradually removed over the length of the taper. Another gradual transition involving via holes brings the top ground planes closer to the microstrip line to form a regular CPW.

After the initial design, a fine optimization in HFSS (Ansys' High Frequency Structure Solver) is performed to improve overall radiation characteristics and input return loss. The final dimensions of all three designs in this paper are summarized in Table I. Note that the feeding CPW impedance differs from 50Ω (cf. last row of Table I) due to size limitations of available CPW test fixtures. Their effect has been calibrated out as described in Section IV. As frequency increases, the substrate thickness must be reduced for satisfactory performance of the ALTSA and the CPW feed. Thus, the 21–31-, 41–61-, and 90–120-GHz ALTSAs are designed on 20-, 10-, and 5-mil substrates, respectively (cf. Table I).

## III. Results

This section presents the results obtained from the design process outlined in the previous section. Note that in addition to the dimensions presented in Table I, the following substrate parameters are considered in the simulations: $\varepsilon_r = 2.94$, $\tan\delta = 0.0012$, metallization thickness $t = 17.5$ $\mu$m, and conductivity $\sigma = 5.8 \times 10^7$ S/m.

The input reflection coefficient (in decibels) of the 41–61-GHz ALTSA is shown in Fig. 2, along with its gain, as simulated with the frequency-domain solver HFSS and the time-domain solver of CST (Computer Simulation Technology's Microwave Studio). The input return loss is better than 20 dB over the entire 20-GHz frequency range, which is attributed to a very good match between the new CPW feed and the SIW as well as between the SIW and the ALTSA. Note that over a narrow frequency range (around 49 GHz), return loss values in excess of 30 dB can be obtained. The gain is better than 13.5 dB at 41 GHz and increases to 14.9 at the end of the band. Overall, the gain is reasonably flat over the entire band, as evidenced by both CST and HFSS, with the CST results marginally higher than those of HFSS.

Radiation pattern examples of this antenna are shown in Fig. 3 for four different frequencies. Over the width of the main beam, results obtained from HFSS and CST are generally in good agreement. For the E-plane beamwidth, the agreement between HFSS and CST results is very good. At the lower frequency end, the H-plane beamwidth in HFSS is predicted a little wider than that in CST. This discrepancy reduces

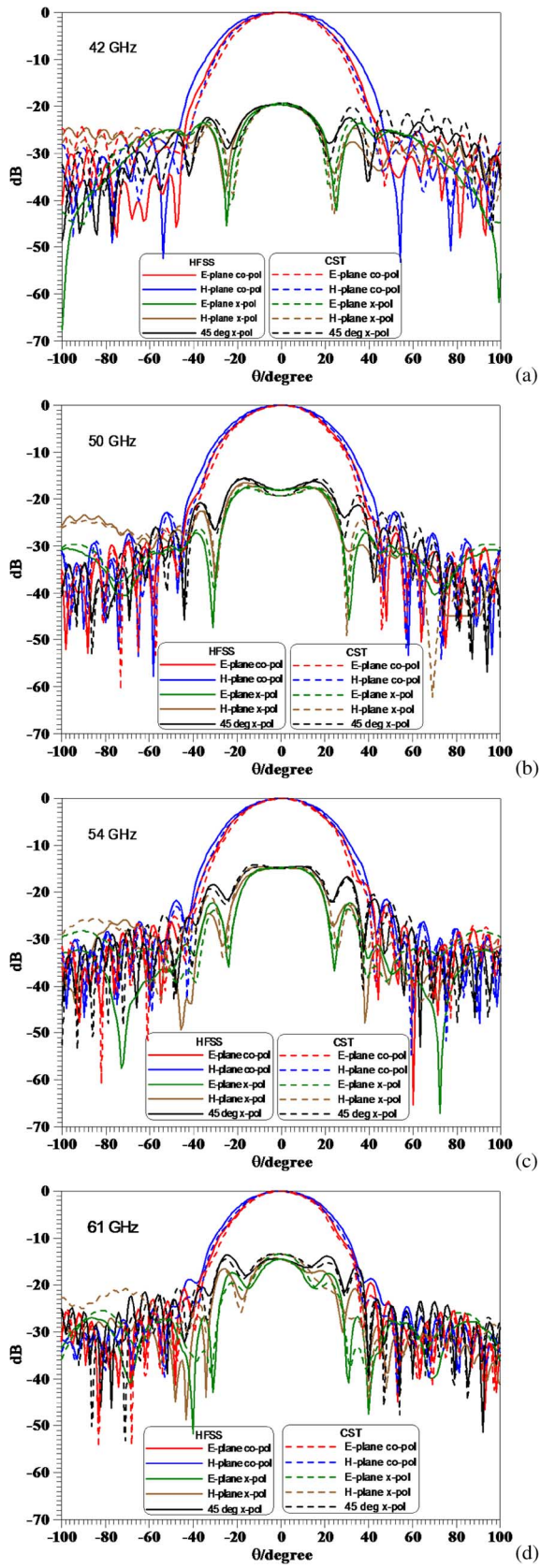


Fig. 3. Radiation patterns of the 41–61-GHz ALTSA and comparison between HFSS and CST at (a) 42 GHz, (b) 50 GHz, (c) 54 GHz, and (d) 61 GHz.

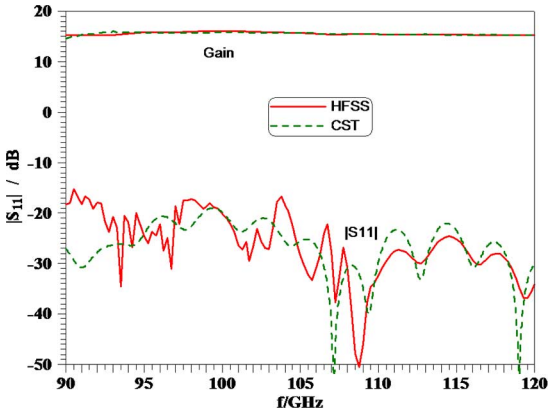


Fig. 4. Input reflection coefficient and gain in decibels of the 90–120-GHz ALTSA and comparison between HFSS and CST.

with increasing frequency, as does the actual beamwidth, as expected. The pattern symmetry is very good over the entire frequency range. Also expected is the fact that over such a wide bandwidth, cross-polarization levels increase with frequency. They are at 20 dB at 42 GHz [Fig. 3(a)] and reduce to 13.3 dB at 61 GHz [Fig. 3(d)]. Note that the maximum cross-polarization level in the 45° cut is only marginally higher than those in the principal planes [Fig. 3(b)–(d)].

The respective performances for the 90–120-GHz ALTSA are shown in Fig. 4 (reflection coefficient and gain) and Fig. 5 (radiation patterns).

The return loss in Fig. 4 is better than 15 dB up to 104 GHz and improves to better than 22 dB beyond 104.5 GHz as confirmed by both HFSS and CST. As previously noticed, this performance can be considerably enhanced over a narrow band (e.g. around 107–110 GHz). The maximum gain variation is only 0.7 dB over the entire band with values between 14.6 dB at 90 GHz and 15.3 dB at 120 GHz by CST. The HFSS data is in excellent agreement.

The radiation patterns of the 90–120-GHz ALTSA in Fig. 5 demonstrate the same trends as observed for those of the 41–61-GHz antenna. The beam symmetry in the H-plane is good but that in the E-plane displays a slight ripple effect towards higher frequencies and positive $\theta$ values, both in CST and HFSS [Fig. 5(b)–(d)]. A similar trend is observed for the 41–61-GHz ALTSA in Fig. 3(c) and (d). However, such effects occur usually below the 10-dB level, and thus are not of primary concern in our designs.

The cross-polarization levels are around 19 dB (HFSS) and 16 dB (CST) at 91 GHz [Fig. 5(a)]. This difference between the two field solvers seems significant but it disappears as frequency increases to 103 GHz and beyond [Fig. 5(b)–(d)]. Cross-polarization levels reduce to 15 dB at 120 GHz with CST and HFSS being in good agreement. Note that the difference in cross-polarization variation (4 dB according to HFSS) across the band is smaller than that for the 41–61-GHz ALTSA (6.5 dB), which is due to the fact that the percentage bandwidth is reduced from 38% at 51 GHz to 28% at 105 GHz.

## IV. Measurements

For verification of the above results, a prototype ALTSA was manufactured according to dimensions in Table I for operation between 21 and 31 GHz. A photograph of the prototype, including the CPW test fixture, is shown in Fig. 6.

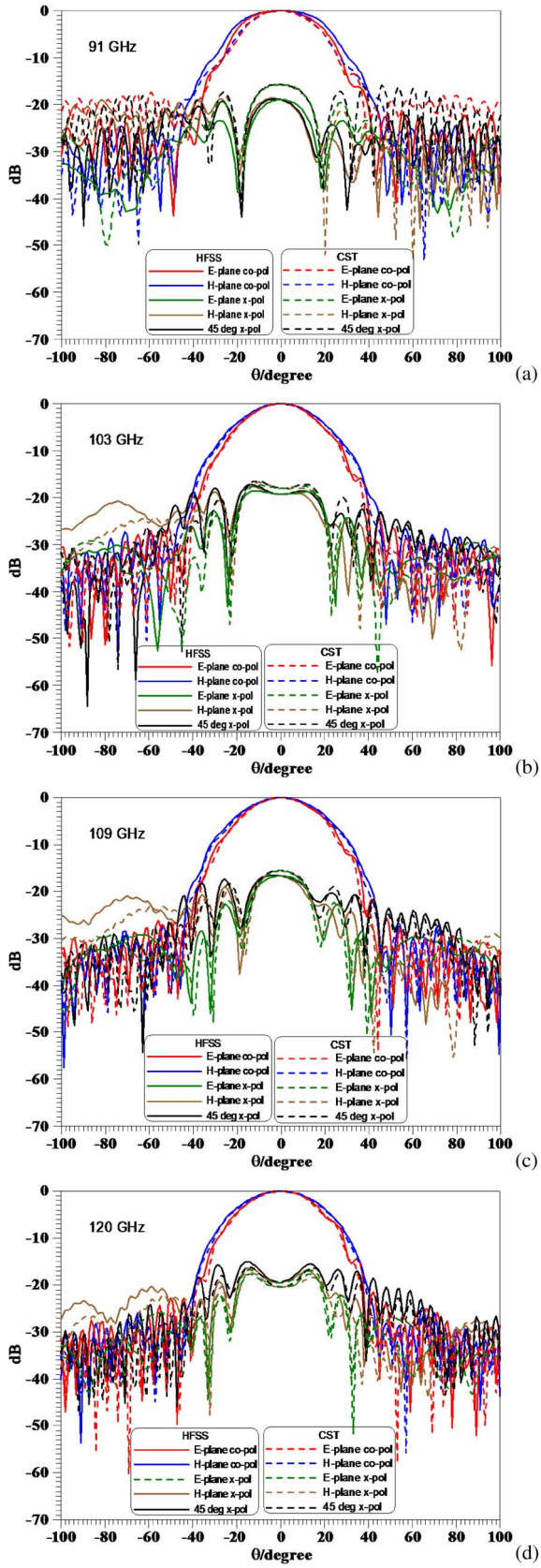


Fig. 5. Radiation patterns of the 90–120-GHz ALTSA and comparison between HFSS and CST at (a) 91 GHz, (b) 103 GHz, (c) 109 GHz, and (d) 120 GHz.

In order to eliminate the effects of the coaxial-to-test-fixture-to-CPW transitions, and thus de-embed the influence of the

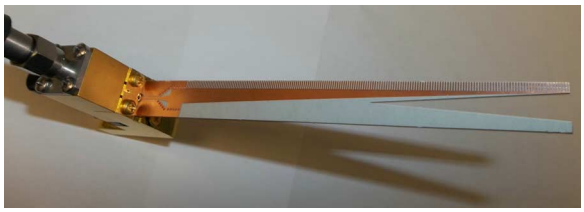

Fig. 6. 21–31-GHz prototype of the SIW-based ALTSA with broadband CPW feed and CPW test fixture.

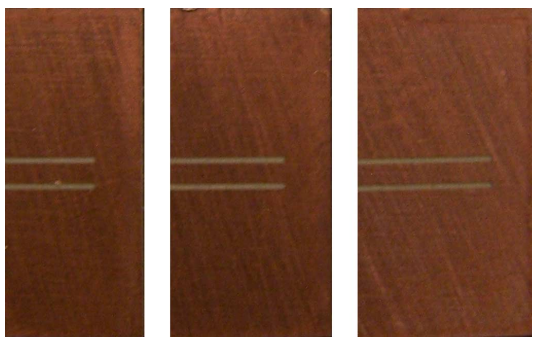

Fig. 7. Triple-short CPW calibration standards to de-embed the effects of the coaxial-to-test-fixture-to-CPW transitions in Fig. 6.

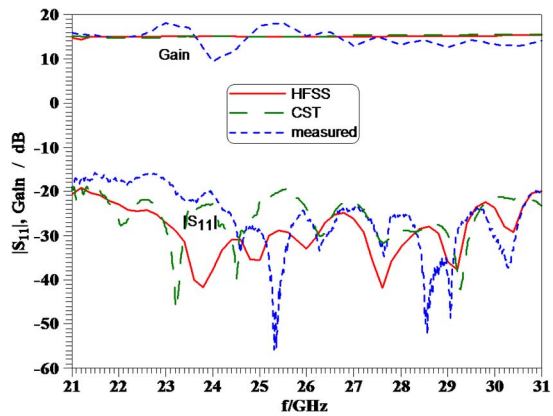


Fig. 8. Comparison between simulations (HFSS and CST) and measurement for input reflection coefficient and gain in decibels of the 21–31-GHz ALTSA prototype.

different impedance levels as stated in Section II, a triple-short (SSS) calibration procedure is used [31]. This technique calls for three shorts of increasing lengths $L_1, L_2, L_3$ such that their reflected electrical lengths, $2\beta L_n$ in degrees, satisfy the conditions

$$20^\circ < 2\beta(L_2 - L_1) < 90^\circ \quad (5)$$

$$20^\circ < 2\beta(L_3 - L_2) < 90^\circ \quad (6)$$

and

$$20^\circ < 2\beta(L_3 - L_1) < 160^\circ \quad (7)$$

where $\beta$ is the phase constant of the CPW at midband frequency. In order to account for the connection to the test fixture, a constant length of 1.5 mm was added to all three lines. Fig. 7 shows photographs of the three calibration standards used.

Radiation pattern measurements are performed with a test antenna, and gain calibration is achieved by replacing the ALTSA with a standard-gain horn and computing the on-axis ALTSA gains [32]. For the frequency range of 21–31 GHz, two standard-gain horns, K- and Ka-band, are required.

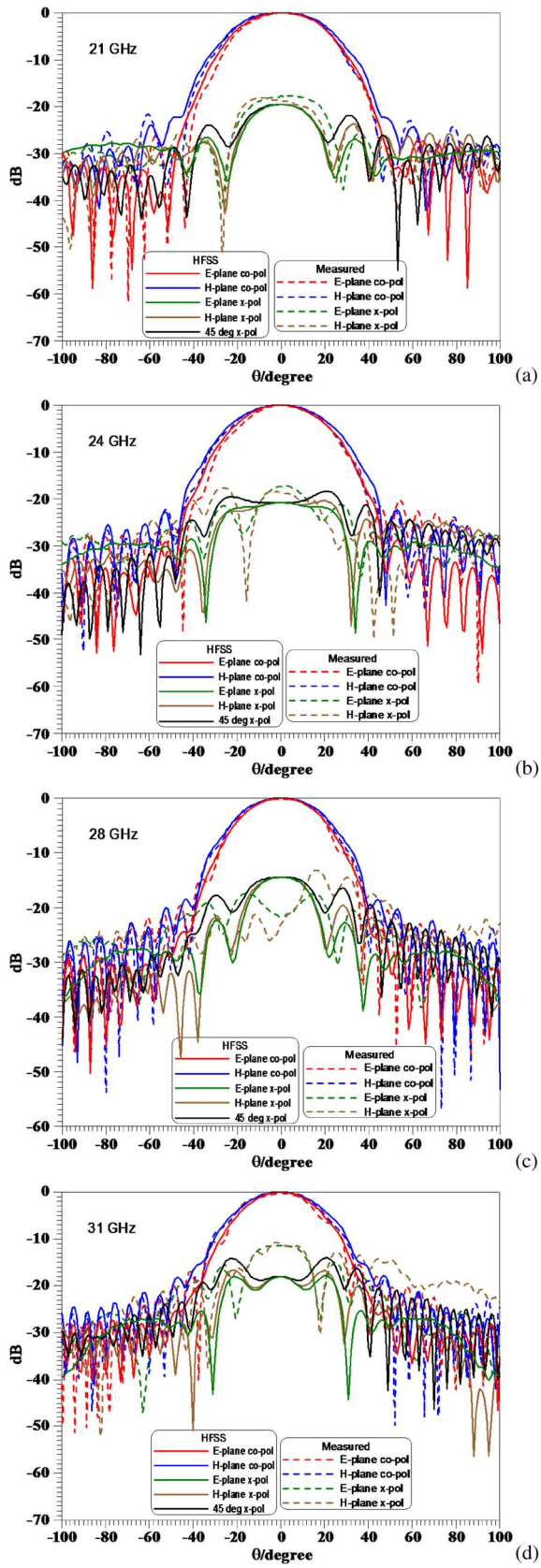


Fig. 9. Comparison between measured and computed radiation patterns of the 21–31-GHz ALTSA at (a) 21 GHz, (b) 24 GHz, (c) 28 GHz, and (d) 31 GHz.

Fig. 8 shows measured and simulated reflection coefficients and gain performances. The general agreement is very good and validates the new combined SIW-CPW feed strategy as well as the design process outlined in Section II. The measured return loss is better than 15 dB over the entire frequency range and better than 20 dB between 24 and 31 GHz. It is noted that the reflection coefficient computed by CST is in slightly better agreement with measurements than that of HFSS and that the gain computations of HFSS and CST are in excellent agreement. The measured gain above 26 GHz is only slightly lower than predicted—as one would expect from the non-ideal measurement setup. In the 21–26-GHz range, however, some inconsistencies in the bore sight E-plane measurements have been observed with respect to those in the H-plane. They have been eliminated in the radiation pattern measurements of Fig. 9(a) and (b) by normalizing the entire set of E-plane measurements to the maximum. However, they do show up as the rippled performance in the gain measurements between 21 and 26 GHz in Fig. 8.

The agreement in the co-polarized E-plane and H-plane pattern measurements in Fig. 9 is very good. The measured half-power beamwidth varies only very slightly—between 36° at 21 GHz and 33° at 31 GHz.

The measured cross-polarization values follow the trends of those demonstrated for the 41–61-GHz and 90–120-GHz ALTSAs; however, their levels are increased compared to those in the simulations. Measured cross-polarization varies between 17.5 dB (simulated value of 19.5 dB) at 21 GHz and 10.8 dB (simulated value of 14 dB) at 31 GHz. However, since 45○ cross-polarization cuts could not be measured, the worst-case cross-polarization measurement of 10.8 dB at 31 GHz might thus increase by approximately 1 dB. This value is based on the simulations of the 41–61- and 90–120-GHz designs in Figs. 3(d) and 5(d), respectively, where the 45° cross-polarization levels come out approximately 1 dB higher than those in the principal planes.

## V. Conclusions

The proposed new combined SIW and CPW feeds for ALTSA designs present a viable option for millimeter-wave broadband printed-circuit antennas in phased array and focal-plane imaging systems. The three designs introduced for 21–31, 41–61, and 90–120 GHz demonstrate nearly flat gain, almost constant beamwidth, and cross-polarization levels comparable with similar ALTSAs. The new CPW feed, which is more appropriate than microstrip at millimeter-wave frequencies, achieves an excellent broadband match to the SIW and ALTSA and eliminates the requirement for air bridges in direct CPW-to-TSA connections. Simulated performances in HFSS and CST are validated by measurements that have verified the predicted beamwidth, return loss, and gain performance. The general trend of increasing cross-polarization with frequency is also verified. However, a maximum difference of 4 dB between simulation and measurement occurs at the end of the band.

## Acknowledgment

The authors would like to thank T. Antonescu of the Poly-Grames Research Center for manufacturing the ALTSA prototype and M. Thibault, also of Poly-Grames, for antenna setup and measurements. Moreover, the authors appreciate the advice of Dr. S. Claude, Herzberg Institute of Astrophysics, Victoria, BC, Canada, in the early stages of the ALTSA design.

## References

[1] P. J. Gibson, "The Vivaldi aerial," in *Proc. 9th Eur. Microw. Conf.*, Brighton, U.K., Jun. 1979, pp. 101–105.
[2] K. S. Yngvesson, D. H. Schaubert, T. L. Korzeniowski, E. L. Kollberg, T. Thungren, and J. F. Johansson, "Endfire tapered slot antennas on dielectric substrates," *IEEE Trans. Antennas Propag.*, vol. 33, pp. 1392–1400, Dec. 1985.
[3] K. S. Yngvesson, T. L. Korzeniowski, Y. S. Kim, E. L. Kollberg, and J. F. Johansson, "The tapered slot antenna—A new integrated element for millimeter wave applications," *IEEE Trans. Microw. Theory Tech.*, vol. 37, pp. 365–374, Feb. 1989.
[4] H. Holter, T.-H. Chio, and D. H. Schaubert, "Experimental results of 144-element dual-polarized endfire tapered-slot phased arrays," *IEEE Trans. Antennas Propag.*, vol. 48, pp. 1707–1718, Nov. 2000.
[5] B. Veidt, G. J. Hovey, T. Burgess, R. J. Smegal, R. Messing, A. G. Willis, A. D. Gray, and P. E. Dewdney, "Demonstration of a dual-polarized phased-array feed," *IEEE Trans. Antennas Propag.*, vol. 59, pp. 2047–2057, Jun. 2011.
[6] J. B. Rizk and G. M. Rebeiz, "Millimeter-wave Fermi tapered slot antennas on micromachined silicon substrates," *IEEE Trans. Antennas Propag.*, vol. 50, pp. 379–383, Mar. 2002.
[7] H. J. Tang, W. Hong, G. Q. Yang, and J. X. Chen, "Silicon based THz antenna and filter with MEMS process," in *Proc. Int. Workshop Antenna Technology (iWAT)*, Hong Kong, Mar. 2011, pp. 148–151.
[8] S.-G. Kim and K. Chang, "Ultra wideband exponentially tapered antipodal Vivaldi antennas," in *IEEE Int. Symp. Dig.*, Monterey, CA, USA, Jun. 2004, pp. 2273–2276.
[9] M. Sun, X. Qing, and Z. N. Chen, "60-GHz antipodal Fermi antenna on PCB," in *Proc. EuCAP*, Rome, Italy, Apr. 2011, pp. 3264–3267.
[10] J. Bai, S. Shi, and D. W. Prather, "Modified compact antipodal Vivaldi antenna for 4–50-GHz UWB application," *IEEE Trans. Microw. Theory Tech.*, vol. 59, pp. 1051–1057, Apr. 2011.
[11] K. Sawaya, H. Sato, Y. Wagatsuma, and K. Mizuno, "Broadband Fermi antenna and its application to mm-wave imaging," in *Proc. 2nd Eur. Conf. Antennas Propag. (EuCAP)*, Edinburgh, U.K., Nov. 2007, pp. 1–6.
[12] D.-C. Chang, B.-H. Zeng, and J.-C. Liu, "Modified antipodal Fermi antenna with piecewise-linear approximation and shaped-comb corrugation for ranging applications," *IET Microw. Antennas Propag.*, vol. 4, pp. 399–407, Mar. 2010.
[13] H. Sato, Y. Takagi, and K. Sawaya, "High gain antipodal Fermi antenna with low cross polarization," *IEICE Trans. Commun.*, vol. E94-B, pp. 2292–2297, Aug. 2011.
[14] Y. Cassivi, L. Perregrini, P. Arcioni, M. Bressan, K. Wu, and G. Conciauro, "Dispersion characteristics of substrate integrated rectangular waveguide," *IEEE Microw. Wireless Compon. Lett.*, vol. 12, pp. 333–335, Sep. 2002.
[15] I. Wood, D. Dousset, J. Bornemann, and S. Claude, "Linear tapered slot antenna with substrate integrated waveguide feed," in *IEEE AP-S Int. Symp. Dig.*, Honolulu, HI, Jun. 2007, pp. 4761–4764.
[16] Z. C. Hao, W. Hong, J. X. Chen, X. P. Chen, and K. Wu, "A novel feeding technique for antipodal linearly tapered slot antenna array," in *IEEE MTT-S Int. Microwave Symp. Dig.*, Long Beach, CA, USA, Jun. 2005, pp. 1641–1643.
[17] Y. J. Cheng, W. Hong, and K. Wu, "Design of a monopulse antenna using a dual V-type linearly tapered slot antenna (DVLTSA)," *IEEE Trans. Antennas Propag.*, vol. 56, pp. 2903–2909, Sep. 2008.
[18] L. Bin, D. Liang, and J. C. Zhao, "The research of broadband millimeter-wave Vivaldi array antenna using SIW technique," in *Proc. ICMMT*, Chengdu, China, May 2010, pp. 997–1000.
[19] D.-G. Yoon, Y.-P. Hong, Y.-J. An, J.-S. Jang, U.-Y. Pak, and J.-G. Yook, "High-gain planar tapered slot antenna for Ku-band applications," in *Proc. Asia-Pacific Microw. Conf.*, Yokohama, Japan, Dec. 2010, pp. 1914–1917.
[20] I. Wolff, "Design rules and realisation of coplanar circuits for communication applications," in *Proc. Eur. Microw. Conf.*, Madrid, Spain, Sep. 1993, pp. 36–41.
[21] S. Iordanescu, G. Bartolucci, S. Simion, and M. Dragoman, "Coplanar waveguide stub/filters on thin membranes and standard substrates," in *Proc. Int. Semicond. Conf.*, Sinaia, Romania, Oct. 1997, vol. 2, pp. 357–360.
[22] S. Lin, A. Elsherbini, S. Yang, A. Fathy, A. Kamel, and A. Elhennawy, "Experimental development of a circularly polarized antipodal tapered slot antenna using SIW feed printed on thick substrate," in *IEEE AP-S Int. Symp. Dig.*, Honolulu, HI, USA, Jun. 2007, pp. 1533–1536.

[23] S. Yang, A. Elsherbini, S. Lin, A. E. Fathy, A. Kamel, and H. Elhennawy, "A highly efficient Vivaldi antenna array design on thick substrate and fed by SIW structure with integrated GCPW feed," in *2007 IEEE AP-S Int. Symp. Dig.*, Honolulu, HI, USA, June 2007, pp. 1985–1988.
[24] F. Taringou and J. Bornemann, "New substrate-integrated to coplanar waveguide transition," in *Proc. 41st Eur. Microw. Conf.*, Manchester, U.K., Oct. 2011, pp. 428–431.
[25] W. Grammer and K. S. Yngvesson, "Coplanar waveguide transitions to slotline: Design and microprobe characterization," *IEEE Trans. Microw. Theory Tech.*, vol. 41, pp. 1653–1658, Sep. 1993.
[26] K.-P. Ma and T. Itoh, "A new broadband coplanar waveguide to slotline transition," in *IEEE MTT-S Int. Microwave Symp. Dig.*, Denver, CO, USA, Jun. 1997, pp. 1627–1630.
[27] F. Taringou and J. Bornemann, "Return-loss investigation of the equivalent width of substrate-integrated waveguide circuits," in *Proc. IEEE MTT-S Int. Microw. Workshop Series on Millimeter Wave Integrat. Technol.*, Barcelona, Spain, Sep. 2011, pp. 703–706.
[28] J. Zucker, "Surface- and leaky-wave antennas," in *Antenna Engineering Handbook*, H. Jasik, Ed. New York, NY, USA: McGraw-Hill, 1961.
[29] S. Sugawara, Y. Maita, K. Adachi, K. Mori, and K. Mizuno, "A mm-wave tapered slot antenna with improved radiation pattern," in *IEEE MTT-S Int. Microw. Symp. Dig.*, Denver, CO, USA, Jun. 1997, pp. 959–962.
[30] D. Deslandes, "Design equations for tapered microstrip-to-substrate integrated waveguide transitions," in *IEEE MTT-S Int. Microw. Symp. Dig.*, Anaheim, CA, USA, May 2010, pp. 704–704.
[31] *"Calibration and Measurement Guide*—Version 1.5.0—VectorStar MS4640A Series Microwave Vector Network Analyzers*,"* Anritsu Company, Morgan Hill, CA, USA, Aug. 2011.
[32] C. A. Balanis*, Antenna Theory-Analysis and Design*. Hoboken, NJ, USA: Wiley, 2005, pp. 1033–1034.

**Farzaneh Taringou** (S'10) received the B.Sc. and M.A.Sc. degrees from Isfahan University of Technology, Esfahan, Iran, and Ecole Polytechnique de Montreal, Montreal, QC, Canada, in 2005 and 2008, respectively.

She is currently working towards the Ph.D. degree at the University of Victoria, Victoria, Canada, in the area of substrate integrated waveguide technology.

**David Dousset** received the Dipl.-Ing degree in electrical engineering from the Polytech Nantes, Nantes, France, in 2000 and the Ph.D. degree from École Polytechnique de Montréal, Montréal, QC, Canada, in 2010.

In September 2010, he joined the Poly-Grames Research Center, Montréal, QC, Canada, which is affiliated with the École Polytechnique de Montréal. His current research interests include designs of antennas and passive and active components in the millimeter-wave frequency range combined with low-loss substrate integrated circuit (SIC) technology.

**Jens Bornemann** (M'87–SM'90–F'02) received the Dipl.-Ing. and the Dr.-Ing. degrees, both in electrical engineering, from the University of Bremen, Bremen, Germany, in 1980 and 1984, respectively.

From 1984 to 1985, he was a consulting engineer. In 1985, he joined the University of Bremen, Bremen, Germany, as an Assistant Professor. Since April 1988, he has been with the Department of Electrical and Computer Engineering, University of Victoria, Victoria, BC, Canada, where he became a Professor in 1992. From 1992 to 1995, he was a Fellow of the British Columbia Advanced Systems Institute. In 1996, he was a Visiting Scientist at Spar Aerospace Limited (now MDA Space), Ste-Anne-de-Bellevue, QC, Canada, and a Visiting Professor at the Microwave Department, University of Ulm, Ulm, Germany. From 1997 to 2002, he was a Co-Director of the Center for Advanced Materials and Related Technology (CAMTEC), University of Victoria. In 2003, he was a Visiting Professor at the Laboratory for Electromagnetic Fields and Microwave Electronics, ETH Zurich, Switzerland. He has coauthored *Waveguide Components for Antenna Feed Systems—Theory and Design* (Artech House, 1993) and has authored or coauthored more than 250 technical papers. His research activities include RF/wireless/microwave/millimeter-wave components and systems design, and field-theory-based modeling of integrated circuits, feed networks and antennas.

Dr. Bornemann served as an Associate Editor of the IEEE TRANSACTIONS ON MICROWAVE THEORY AND TECHNIQUES in the area of Microwave Modeling and CAD from 1999 to 2002. From 1999 to 2009, he served on the Technical Program Committee of the IEEE MTT-S International Microwave Symposium. He is a Registered Professional Engineer in the Province of British Columbia, Canada. He is a Fellow of the Canadian Academy of Engineering (CAE) and serves on the editorial advisory board of the *International Journal of Numerical Modelling*.

**Ke Wu** (M'87–SM'92–F'01) received the B.Sc. degree (with distinction) in radio engineering from Nanjing Institute of Technology (Now Southeast University), Nanjing, China, in 1982 and the D.E.A. degree in electronics and Ph.D. degree (with distinction) in optics, optoelectronics, and microwave engineering from the Institut National Polytechnique de Grenoble (INPG), Grenoble, France, in 1984 and 1987, respectively.

He is a Professor of electrical engineering and the Tier-I Canada Research Chair in radio frequency and millimeter-wave engineering with the École Polytechnique de Montréal, Montréal, QC, Canada. He holds the first Cheung Kong endowed chair professorship (visiting) at Southeast University, the first Sir Yue-Kong Pao chair professorship (visiting) at Ningbo University, and an honorary professorship with the Nanjing University of Science and Technology, the Nanjing University of Post Telecommunication, and the City University of Hong Kong, China. He has been the Director of the Poly-Grames Research Center and the founding Director of the Center for Radiofrequency Electronics Research of Quebec (Regroupement stratégique of FRQNT). He has also held guest and visiting professorship with many universities around the world. He has authored or coauthored over 860 referred papers and a number of books, book chapters, and patents. He has served on the editorial or review boards of many technical journals, transactions, and letters as well as scientific encyclopedia including as editor and guest editor. His current research interests involve substrate integrated circuits, antenna arrays, advanced computer-aided design and modeling techniques, wireless power transmission, and development of low-cost RF and millimeter-wave transceivers and sensors for wireless systems and biomedical applications. He is also interested in the modeling and design of microwave photonic circuits and systems.

Dr. Wu is a Fellow of the Canadian Academy of Engineering (CAE) and a Fellow of the Royal Society of Canada (The Canadian Academy of the Sciences and Humanities) and a member of Electromagnetics Academy, Sigma Xi, and the URSI. He has held key positions in and has served on various panels and international committees, including the chair of technical program committees, international steering committees, and international conferences or symposia. In particular, he was the General Chair of the 2012 IEEE Microwave Theory and Techniques Society (IEEE MTT-S) International Microwave Symposium. He is currently the Chair of the joint IEEE chapters of MTTS/APS/LEOS in Montreal, QC, Canada. He is an elected IEEE MTT-S AdCom member for 2006–2015 and served as Chair of the IEEEMTT-S Member and Geographic Activities (MGA) Committee. He was the recipient of many awards and prizes including the first IEEE MTT-S Outstanding Young Engineer Award, the 2004 Fessenden Medal of the IEEE Canada, and the 2009 Thomas W. Eadie Medal of the Royal Society of Canada. He was an IEEE MTT-S Distinguished Microwave Lecturer from January 2009 to December 2011.